NUMERICAL STUDY OF RESONANT CHARACTERISTICS FOR MATERIALS EMBEDDED IN PARALLEL PLATE WAVEGUIDE CAVITIES

Shinichiro OHNUKI and Takashi HINATA
Department of Electrical Engineering, College of Science and Technology, Nihon University
1-8 Surugadai, Kanda, Chiyoda-ku, Tokyo, 101-8308 Japan
E-mail: hinata@ele.cst.nihon-u.ac.jp

1. Introduction

The analysis of electromagnetic scattering by open-ended structures plays an important role in radar cross section (RCS) prediction and reduction. As a fundamental open-ended scatterer, a parallel plate waveguide cavity is considered analytically and numerically [1]-[3]. This paper shows a numerical analysis of an electromagnetic scattering by a parallel plate waveguide cavity whose interior region is separated into two areas by inserted plates (Fig.1). The left-hand side cavity is filled with a material whose constant is expressed by (ε_1, μ_1). The constant in other two regions, the right-hand side cavity and the outside of the cavity, is (ε_0, μ_0). Our goal is to clarify RCS characteristics for the internal coupling problems between two areas. In our previous work for the case without material loading [4][5], we discussed the dependence of the RCS characteristics on the size of the iris and the position of the iris. In this paper, the further investigation for the E -polarized case and the H -polarized case is carried out and we will show the resonant properties more clearly for changing the material constants. The analytical technique is the Point Matching Method (PMM) taking into account the edge condition of the conducting rectangular walls [3]-[5].

2. Formulation

A parallel plate waveguide cavity is assumed to be uniform along the z -axis ($\partial / \partial z = 0$) with the cross section of $2a \times 2b$ as shown in Fig.1. The internal area is divided into two regions by

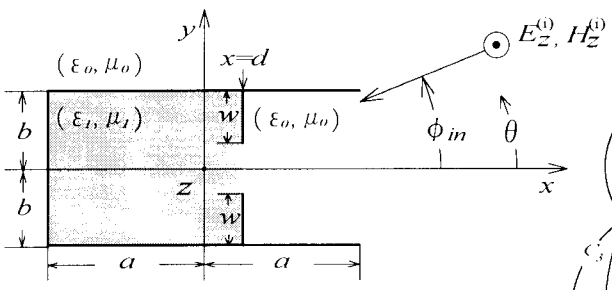

Fig.1 Geometry and coordinate system of a parallel plate waveguide cavity with an iris

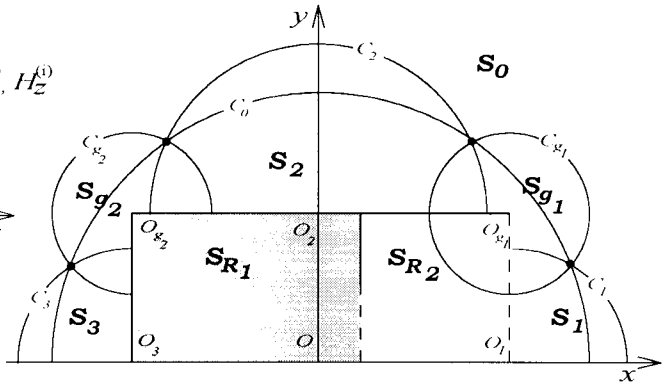

Fig.2 Separation of a physical space for PMM

the plates which are placed at $x = d$ and $b - w \le |y| \le b$. The rectangular cylinder wall and inner plates are assumed to be infinitely thin and perfectly conducting. The following formulation shows an example for the H-polarized case. The time dependence is assumed to be $\exp(j\omega t)$ and suppressed throughout the formulation. The incident plane wave impinges on the scatterer with the angle of incidence ϕ_{in} (Fig.1). Considering the symmetry of the scatterer about x-axis, we can decompose the incident wave into the even-phase component ($p = 0$) and the odd-phase component ($p = 1$). Therefore, the incident wave $H_z^{(i)}[p]$ can be expressed by :

$$H_z^{(i)}[p] = 1/2[\exp\{jkr\cos(\theta - \phi_{in})\} + (-1)^p \exp\{jkr\cos(\theta + \phi_{in})\}] \tag{1}$$

where $k := \omega\sqrt{\varepsilon_0 \mu_0}$, ε_0 : permittivity of the vacuum, μ_0 : permeability of the vacuum.

It suffices to consider the electromagnetic fields in the upper half side of the plane ($0 \le \theta \le \pi$).

In our PMM, the most important matter is to decompose the whole physical space into a finite number of sub-domains in which electromagnetic fields can be expanded by a sum of the separation-variable solutions of Helmholtz equation. In order to accomplish this purpose, the eight regions in Fig.2 are introduced for the scatterer. We cite the following examples, regions S_0 and S_{R_1}, to show how to divide the physical space and expand electromagnetic fields.

(A) Region S_0 : Outside the circle C_0

The scattered wave $H_z^{(S_0)}[p]$, satisfying Maxwell's equations and the radiation condition, is approximated by a finite sum of modes in the cylindrical coordinates $O(r,\theta)$:

$$H_z^{(S_0)}[p] = \sum_{n=p}^{N-1} A_n^{(p)} H_n^{(2)}(kr)\cos\left(n\theta - \frac{\pi}{2}p\right) \tag{2}$$

N : the truncation mode number, $H_n^{(2)}(\bullet)$: Hankel function of the second kind of order n.

(B) Region S_{R_1} : Left-hand side cavity ($-a \le x \le d, |y| \le b$)

The magnetic field $H_z^{(S_{R1})}[p]$ can be expanded by using the waveguide mode:

$$H_z^{(S_{R1})}[p] = \sum_{n=0}^{L_1-1}\left[B_{2n+p}^{(p)}\cos\left\{\gamma_{2n+p}^{(1)}(x+a)\right\}\cos\left\{\frac{(2n+p)\pi}{2b}(y+b)\right\}\right] \tag{3}$$

$$\gamma_n^{(1)} := \sqrt{k_1^2 - \left(\frac{n\pi}{2b}\right)^2}, \qquad k_1 := \omega\sqrt{\varepsilon_1 \mu_1}. \tag{4}$$

Definition of the other regions and their electromagnetic fields are given by the same method in Ref [4]. All the expansion coefficients in the regions are determined to satisfy the continuity conditions at sampling points which are placed at almost same intervals on the boundaries.

3. Numerical Results

Resonant characteristics which depend upon materials embedded in S_{R_1} are investigated. Geometrical parameters of the scatterer are b/a =1.0, d/a =0.2, w/b =0.9 and the following material constants, ε_r (:= $\varepsilon_1/\varepsilon_0$) and μ_r (:= μ_1/μ_0), are assumed:

(M_1) ε_r =4.0, μ_r =1.0 : solid line

(M_2) ε_r =2.5, μ_r =1.6 : dotted line

(M_3) ε_r =2.0, μ_r =2.0 : dashed line

(M_4) ε_r=1.0, μ_r=4.0 : long-dashed/short-dashed line

Refractive indices for these constants have the same value of $\sqrt{\varepsilon_r \mu_r}$ (=2.0). Therefore we may expect that all the resonant frequencies are the same and half of that for the empty case.

Figure 3 shows the resonant characteristic of $E_{1,1}$ which is assigned as the same as the waveguide mode in S_{R_1}. From the numerical result for the E polarized case, we find slight differences of resonant frequencies among four materials. The resonant frequency for the case of M_1 is half of that for the empty case. Decreasing ε_r from 4.0 to 1.0, the resonant frequency is slightly shifted to higher in ka.

Figure 4 is a plot of the electric field distribution of $E_{1,1}$ inside the cavity. The electric field is mainly concentrated in S_{R_1}, but we can clarify the internal coupling through the iris. For this type of resonance, the resonant frequency depends upon material constants even when the refractive indices have the same value.

Figure 5 shows the RCS in the range of ka=2.03 − 2.06 to investigate the resonant characteristic of $E_{1,2}$. This property is different from that for $E_{1,1}$. All the resonant frequencies have the same value. It means that we can not estimate the constitutions of the materials whose refractive indices are the same. To explain the reason for this characteristic, we show the electric field distribution in Fig.6. From the figure, the internal coupling between two cavities is so weak that the electric field is observed only in S_{R_1} and is subject to the physical condition of S_{R_1}.

Figure 7 shows the RCS in the range of ka=0.10 − 0.40 to investigate Helmholtz resonance (H_{el}) which is a characteristic phenomenon only for the H polarized case. The peak for the case of M_4 is observed at ka=0.20 which is half of that for the empty case. Decreasing μ_r from 4.0 to 1.0, the resonant frequency is shifted to higher in ka and the peak becomes smaller.

Figure 8 is a plot of the magnetic field distribution of H_{el} inside the cavity. The distribution is totally different from those of $E_{1,1}$ in Fig.4 and $E_{1,2}$ in Fig.6. The amplitude is almost uniform both internal regions and the internal coupling is strong through the iris.

4. Conclusion

In this paper, we showed the RCS of a material loaded parallel plate waveguide cavity with an iris. The numerical technique was the point matching method taking into account the edge condition for the conducting enclosure. We discussed the dependence of the cavity resonance on the materials embedded inside the cavity and they were clarified in terms of the internal coupling through the iris.

References

[1]Heyman, E., Friedlander, G. and Felsen, L.B., Proc. IEEE, vol.77, no.5, pp. 780-787, 1989.

[2]Kobayashi, K. and Sawai, A., J. Electromagn. Waves Applic.,vol.6, no.4, pp. 475-512, 1992.

[3]Ohnuki,S., Yamasaki,T.,and Hinata, T.,IEICE Trans.Electron.,vol.E76-C,no.10,pp.1474-1480, 1993.

[4]Ohnuki, S. and Hinata, T., IEICE Trans.Electron.,vol.E81-C,no.12, pp.1875-1880, 1998.

[5]Ohnuki, S. Hinata, T., and Hosono, T., 1999 Int. Symposium on EMC, May 17-21, Tokyo, Japan.

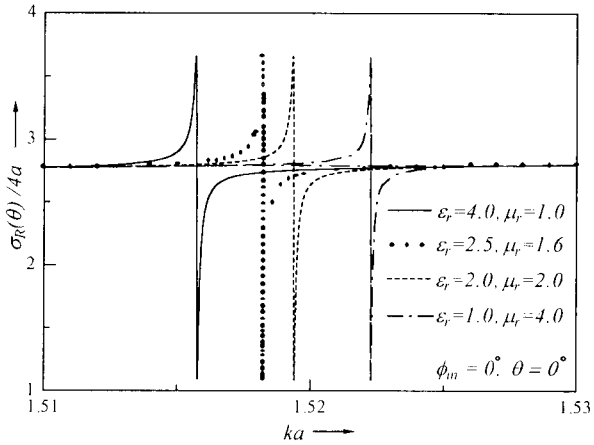

Fig.3 RCS vs. ka – $E_{1,1}$ mode –

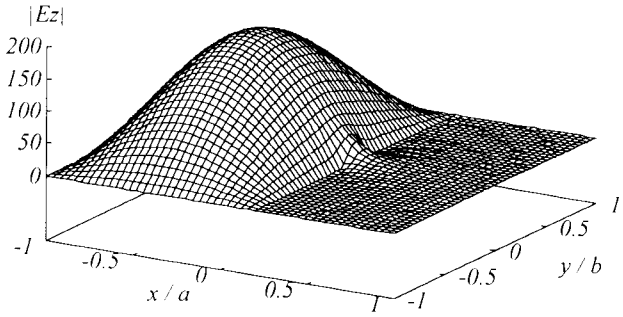

Fig.4 Field distribution of $E_{1,1}$ mode

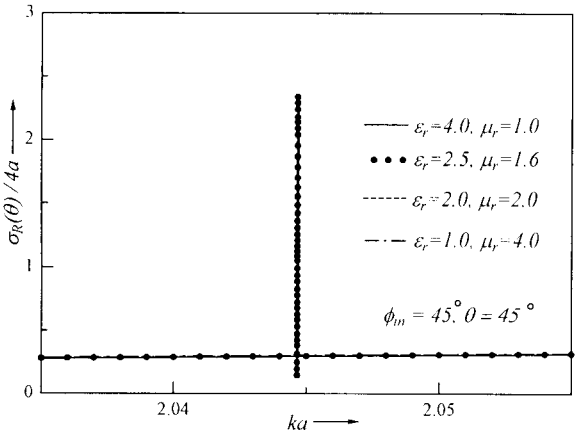

Fig.5 RCS vs. ka – $E_{1,2}$ mode –

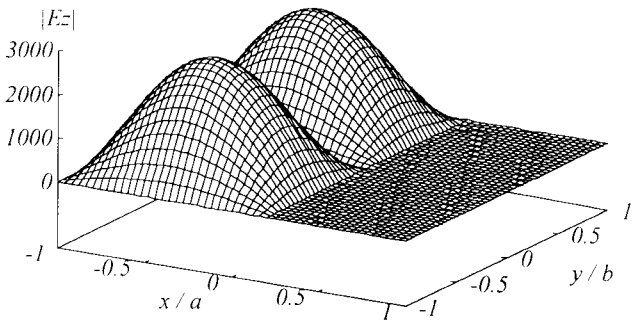

Fig.6 Field distribution of $E_{1,2}$ mode

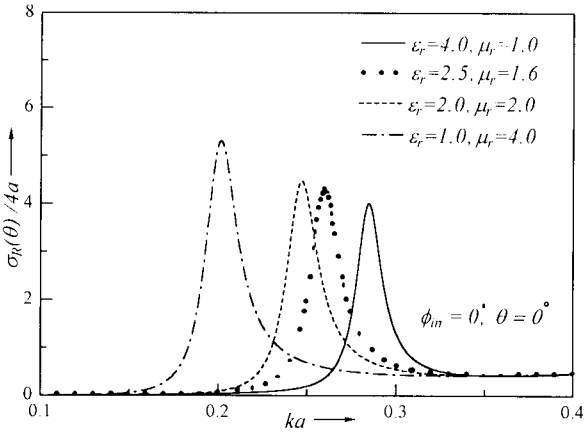

Fig.7 RCS vs. ka – H_{el} –

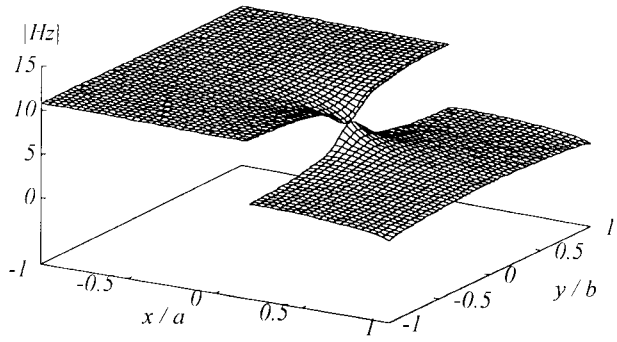

Fig.8 Field distribution of H_{el}